Influence of nanoparticle size on the nonlinear optical properties of magnetite ferrofluids

D. Espinosa, L. B. Carlsson, and A. M. Figueiredo Neto
Instituto de Física, Universidade de São Paulo, Caixa Postal 66318, 05314-970 São Paulo, SP, Brazil

S. Alves
Instituto de Ciências Ambientais, Químicas e Farmacêuticas, Universidade Federal de São Paulo, Diadema, SP, Brazil

(Received 7 May 2013; revised manuscript received 26 July 2013; published 9 September 2013)

The nonlinear index of refraction (n_2) and the two-photon absorption coefficient (β) of water-based ferrofluids made of magnetite nanocrystals of different sizes and with different coatings have been measured through the Z-scan technique, with ultrashort (femtoseconds) laser pulses. Their third-order susceptibility is calculated from the values of n_2 and β. The influence of different particles' coatings and sizes on these nonlinear optical properties are investigated. The values of n_2 and β depend more significantly on the nanoparticles' size than on the particular coating. We observe a decrease of β as the nanoparticles' diameters decrease, although the optical gap is found to be the same for all samples. The results are interpreted considering modifications in the electronic orbital shape due to the particles' nanosize effect.

DOI: 10.1103/PhysRevE.88.032302 PACS number(s): 83.80.Gv, 75.50.Tt, 61.46.Df, 42.65.An

I. INTRODUCTION

Colloidal materials made of magnetic nanoparticles (MNPs) suspended in a liquid carrier are known as ferrofluids or magnetic fluids. The MNPs are made of a magnetic core whose surface is electrically charged or coated with polymeric surfactants to avoid their aggregation. This process leads to the colloidal stability. The magnetic core can be made of magnetite (Fe_3O_4), maghemite (γ-Fe_2O_3), and ferrites ($[M]Fe_2O_4$, where $[M] = Ni^{2+}$, Cu^{2+}, Co^{2+}, Zn^{2+}, Mn^{2+}), among other magnetic solids [1–5]. In the case of magnetite, the crystalline core presents the inverse cubic spinel structure, with the structural formula $(Fe^{3+})[Fe^{2+}Fe^{3+}]O_4$. Here the parentheses indicate the ions in the tetrahedral sites and the square brackets indicate the ions in the octahedral sites [6,7]. Magnetite is a half metal (spin-polarized mixed-valence metal) with a poor dc conductivity (about 0.1% of copper at 23 °C) [8].

Ferrofluids have been employed in electrical and electronic devices—including sensor and actuators—, microelectromechanical and nanoelectromechanical systems (MEMS and NEMS)—including microfluidics and nanofluidics—, biological and biomedical applications, materials science and engineering, and optofluidics [9–14]. In particular, optofluidics is a new area, originating from the convergence of photonics and microfluidics, which combines the fluidity of a liquid (or a colloid) with its optical properties, aiming to develop new devices for new technological applications [15,16]. Magnetic fluids may be very interesting for optofluidic devices due to their remarkable refractive and absorptive nonlinear optical (NLO) properties, tuned by the magnetic field [17–22]. Despite the importance of magnetic fluids applications in optofluidics, only few reports concerning their ultrafast NLO properties are available in the literature [23,24].

Besides the technological appeal, the NLO study of magnetic colloidal systems is also interesting from the fundamental point of view. Since the particles have typical sizes, in general, between 10^{-9} and 10^{-7} m, some of their properties may change when compared to those from the bulk. These nanoscale-size effects (in short, nanosize effects) can be sensitive to little changes in the particles' average diameters. The understanding of the origins and mechanisms of the nanosize effects is a complex challenge of the condensed matter physics nowadays.

In the case of low-order NLO effects, the physical parameters involved in the theoretical formalism are the nonlinear polarizations and susceptibilities [25]. When an external magnetic field is applied to a ferrofluid, the MNPs' permanent magnetic moments tend to align along the field direction; this alignment breaks the material isotropy and the second-order nonlinear susceptibility ($\chi^{(2)}$) has to be considered [26]. Without any applied magnetic field, the magnetic moments are randomly oriented and the ferrofluid is optically isotropic. In this case, the macroscopic $\chi^{(2)}$ was experimentally and theoretically found to be zero [26], as expected in isotropic and centrosymmetric materials [27]. Therefore, the first relevant nonlinear contribution that has to be considered in the calculation of the total index of refraction (n) and absorption (α) of the material is the third-order susceptibility ($\chi^{(3)}$). This is the case of the present work, where the samples are not under an external applied magnetic field.

The parameters that inform about the nonlinear third-order susceptibility of a material are the nonlinear index of refraction (n_2) and absorption (β). These parameters are also named optical Kerr and two-photon absorption (TPA) coefficients, respectively. The total index of refraction and absorption of the material may be written as

$$n = n_0 + n_2 I, \quad \alpha = \alpha_0 + \beta I,$$

where n_0 and α_0 are the linear index of refraction and absorption, respectively, and I is the intensity of the light interacting with the material.

There are some interesting findings about the NLO properties of semiconductor particles (or quantum dots—QDs) in the nanoscale dimensions. Semiconductor CdSe and CdTe colloidal QDs present a two-photon absorption (TPA) coefficient (and its respective cross section) that decreases as the QD's size decreases [28,29]. Some models and mechanisms have been proposed to explain these experimental results: the energy density of TPA transitions decreases as the QD's size decreases,

and TPA also decreases with the increasing of band gap energy, which is expected to occur for smaller particles [30]; the electrons scattering on surface defects become important as the size decreases, resulting in a decreasing in the TPA [31]; and the consideration of the conduction-valence band mixing for smaller particles in the eight-band Pidgeon and Brown effective-mass approximation [32]. The nonlinear refractive index and TPA coefficient of semiconductor Mn-doped ZnSe nanocrystals and semiconductor Si QDs decrease with the decrease in the size of the QDs [33,34]. Semiconductor PbS QDs, however, present an inverse behavior: their TPA increases as the QD size decreases. This result may be due to its unusual band structure [35]. Metallic QDs' third-order susceptibility decreases as their size decreases. This result is mainly due to the saturation of optical transitions between discrete states of conduction electrons [36]. However, for half metallic nanoparticles, such as magnetite, this literature is rare.

In this work, we use the Z-scan technique [37,38] to investigate the refractive and absorptive ultrafast optical nonlinearities of Fe_3O_4 water-based ferrofluids. The contributions of the different coatings to the NLO properties of the magnetic fluid are also investigated. This aspect is important because, on the one hand, this subject is still not very well known and, on the other hand, it is necessary to separate an eventual optical nonlinearity, due to the nanoparticle coating, from that of the magnetite nanoparticle itself.

II. EXPERIMENT

A. Samples

The materials investigated here are commercial ferrofluids (from fluidMAG, Chemicell GmbH) made of single domain magnetite nanoparticles (Fe_3O_4) dispersed in water. The nanoparticles are coated with molecules with hydrophilic regions in contact with water, or have a surface-charge density to avoid the particles' aggregation. The sample labels with their respective coatings are as follows: DXS: dextran sulfate; DX: dextran; UCA: uncoated anionic charged; lipid: phosphatidylcholine; CT: citric acid; amine: aminosilane; chitosan: chitosan; OS: oleic acid. The hydrodynamic diameter of the particles, informed by the manufacturer, is 50 nm for all samples. For all the samples, the volume fraction occupied by the nanoparticles was 2% for the Z-scan, transmission electron microscopy (TEM) and x-ray diffraction (XRD) experiments and 0.003% for the UV-vis spectroscopy experiments.

B. Experimental techniques

1. X-ray diffraction (XRD), transmission electron microscopy (TEM), UV-vis spectroscopy

The XRD experiments were performed on the diffractometer CN4037A1, from Rigaku Corporation, with monochromatic beam (wavelength of 1.5418 Å). The operating voltage and current were 40 kV and 30 mA. The sample was encapsulated in a borosilicate glass capillary (1.5 mm outer diameter, 0.01 mm wall thickness). The distance between the sample and the image plate used to detect the diffraction pattern was 36 mm. The different parts of the setup are arranged in the Laue geometry.

The TEM images were obtained with the LEO906E system (Carl Zeiss Inc.). The operating voltage was 100 kV. For the TEM experiments, the samples were placed on copper grids coated with parlodium-carbon.

For the UV-vis experiments, the samples were placed in 10-mm optical path length quartz cuvettes, positioned in a spectrophotometer with a deuterium tungsten halogen light source DH-2000-BAL, Mikropack GmbH, and spectrometers USB4000, Ocean Optics Inc. The light-wavelength range varied from 270 to 1000 nm. The temperature of the samples in all the experiments was 22 °C.

2. Z-scan

The Z-scan experiment was performed in the open-aperture (OA) and closed-aperture (CA) geometries [38]. The light source used in our system is a femtoseconds pulse-train laser, with frequency of 1 kHz, wavelength of 800 nm, and pulse width of 196 fs. The pulse train is generated by the Ti:sapphire laser (Chameleon Ultra II, Coherent Inc.) at the frequency of 80 MHz and a Pockels cell module (305, Conoptics Inc.) is used to decrease this frequency to 1 kHz. With this procedure we avoid the unwanted spurious thermal effects [24]. A lens with focal distance of 12.5 cm was used to give, at the focal position, the beam waist (w_0) of (25 ± 1) μm [$z_0 = (2.45 \pm 0.25)$ mm], and the on-axis peak intensity (I_0) of (12.4 ± 1.7) GW/cm^2. At each sample position along the z axis, the pulse energy transmitted through the sample was measured by a fast detector (SV2-FC, Thorlabs Inc.). This energy was used to calculate the normalized transmittance (Γ_N), with respect to the pulse energy transmitted when the sample is far from the focus, as a function of z. Samples were encapsulated between glass plates (dimensions $20 \times 10 \times 1$ mm^3) separated by a spacer with thickness (L) of 100 μm. We checked that this type of cell filled with water, without the nanoparticles, does not show any NLO response in our Z-scan setup. More details about the experimental setup may be found in Refs. [24,39]. The temperature of the samples in all the experiments was 22 °C.

III. RESULTS AND DISCUSSION

The x-ray diffraction patterns obtained for all samples present different diffraction peaks. One of them is that corresponding to the magnetite crystallographic planes (311) [40]. This peak was used to calculate the crystalline size of the particles by using the Scherrer's equation [41–43]. The peak broadening is related to the finite (mean) crystalline size of the particles. The diameters of the crystalline magnetite cores obtained with this procedure (D_{XRD}) are presented in Table I.

The diameters obtained by TEM are also shown in Table I. In this case, the TEM images were analyzed and the diameter of approximately 900 nanoparticles was measured, for each sample. A log-normal distribution was fitted to the histogram of the diameters, where the adjustable parameters were the median (D_{TEM}) and standard deviation (σ_{TEM}). We chose the histogram bin width value that results in the best log-normal distribution fitting for each sample, as presented in Table I. D_{XRD}, D_{TEM}, and σ_{TEM} are in agreement with the relation $D_{XRD} \sim D_{TEM} \exp(2.5\sigma_{TEM}^2)$ [44], therefore the XRD diameters are compatible with the TEM diameters. However,

TABLE I. Particles' diameters measured by using XRD and TEM.

Sample label	D_{XRD} (nm)	D_{TEM} (nm)	σ_{TEM} (nm)	bin_{TEM} (nm)
DXS	7.6 ± 0.6	8.2	0.3	1.02
DX	8.3 ± 0.7	9.5	0.3	1.03
UCA	8.6 ± 0.7	8.5	0.4	1.05
Lipid	10.3 ± 0.8	9.6	0.3	1.00
CT	10.9 ± 0.9	11.2	0.3	1.00
Amine	11.6 ± 0.9	10.2	0.4	1.03
Chitosan	15.7 ± 1.3	10.6	0.3	0.95
OS	16.1 ± 1.3	10.7	0.3	1.02

the hydrodynamic diameter of 50 nm, measured through photon correlation spectroscopy (PCS) by the ferrofluids' manufacturer, is different from the values obtained by XRD and TEM. The higher diameter values measured by PCS were also found in some works [45–48] and can be explained as follows. First, the hydrodynamic sizes are expected to be bigger than the bare particle size, because they are defined as the magnetite core diameter plus the coating shell thickness, and the hydration shell thickness around the particle [46,49]. Second, big particles and particle aggregates influence very much the PCS results [45,48]. With these considerations, we chose the diameter values obtained by XRD, which are related to the magnetite core, to investigate the relation between the macroscopic nonlinear optical properties and the microscopic particles' properties.

The absorbance spectra of the ferrofluids investigated in this work are shown in Fig. 1. All the samples are practically transparent to light at the wavelength of $\lambda = 800$ nm, but their linear absorbance increases significantly in the region around $\lambda = 400$ nm. The absorbance values at the ultraviolet range differ from sample to sample, showing some influence of the coating layer. Besides, in the case of our particles' size, the absorbance data may have contributions from the absorption and from the Rayleigh scattering of the light by the particles. The last one is expected to follow a λ^{-4} dependence [50,51]. In this work, we used the absorbance word as a synonym of extinction, i.e., absorption plus scattering.

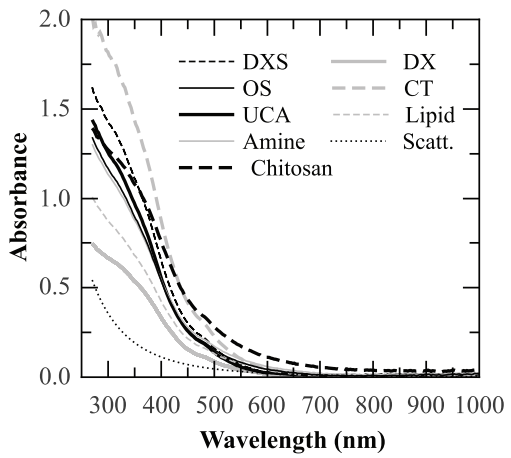

FIG. 1. Absorbance spectra of the investigated ferrofluids. The curve identified by "Scatt." is an estimative to the Rayleigh scattering for the UCA sample.

We estimated the Rayleigh scattering contributions (A_{scat}) to the absorbance data by fitting $A_{scat} = a\lambda^{-4}$ curves to the region between $\lambda = 650$ and $\lambda = 750$ nm, where a is an adjustable parameter. This wavelength region was chosen because the absorbance is minimum there and we have assumed that the absorbance data are due, mainly, to the scattering. If some absorption is present in the 650–750 nm region, the scattering contribution would be even lower. Therefore, our absorbance curve corresponds to the maximum (possible) Rayleigh scattering values. Then, the achieved a value was fixed and the curves were extrapolated to the other regions of the spectrum. We also presented in Fig. 1 the estimated Rayleigh scattering curve for the UCA sample, using this procedure. To check the contribution of the different coatings we measured the linear absorbance spectra of saturated aqueous solutions of citric acid, phosphatidylcholine, and dextran; of chitosan solution in acetic acid; and of pure oleic acid. We verified that these materials absorb light at wavelengths shorter than ~380 nm, and do not absorb at $\lambda \gtrsim 400$ nm. Magnetite nanoparticles absorb light at $\lambda \lesssim 600$ nm, as shown in the spectra of the uncoated sample (UCA) (see Fig. 1). So, the appropriate experimental conditions to investigate the TPA in these ferrofluid samples is to use incident light at $\lambda = 800$ nm, and measure the pulse energy transmitted in the Z-scan experiment.

Figure 2 shows typical experimental data from the CA Z-scan experiments for the samples coated with citric acid

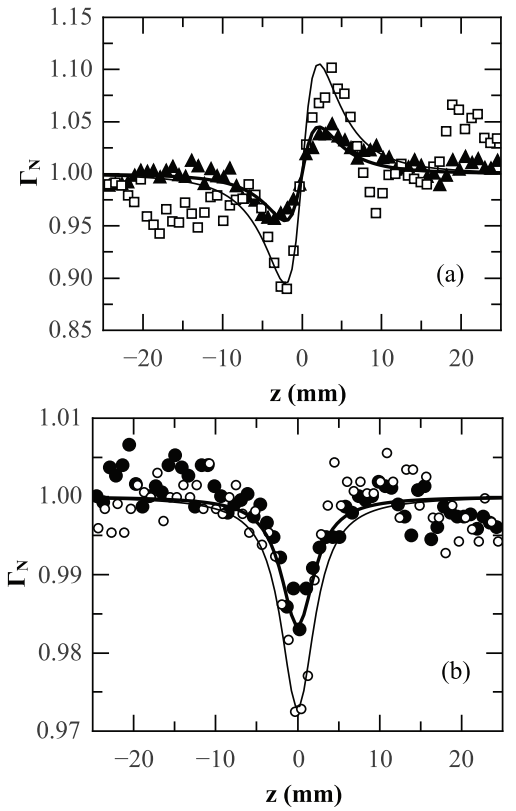

FIG. 2. Typical Z-scan curves of the normalized transmittance as a function of the z position of the sample, incident light with $\lambda = 800$ nm. (a) CA configuration, (▲) CT sample, (□) chitosan sample. Solid lines are fits with Eq. (1); (b) OA configuration, (●) DXS sample, (○) OS sample. Solid lines are fits with Eq. (2).

and chitosan (a), and from the OA Z-scan experiments for the samples coated with dextran and oleic acid (b). To remove the contribution of the nonlinear absorption from the CA Z-scan data, we divided, point by point, the measured values by the OA Z-scan data. Different samples present different amplitudes of the Z-scan signal, for the same experimental conditions. The theoretical framework used to obtain the nonlinear refractive index (n_2) and the TPA coefficient (β) is that developed by Sheik-Bahae *et al.* [38], summarized by Eqs. (1) and (2). These equations describe the behavior of the normalized transmittance as a function of z, in the CA [see Eq. (1)] and OA [see Eq. (2)] Z-scan geometries:

$$\Gamma_{\mathrm{N}}^{\mathrm{CA}}(\gamma) = 1 + \frac{8\pi}{\lambda}\frac{n_2 I_0 L_e \gamma}{(\gamma^2+9)(\gamma^2+1)}, \tag{1}$$

$$\Gamma_{\mathrm{N}}^{\mathrm{OA}}(\gamma) = \sum_{m=0}^{+\infty}\frac{[-\beta I_0 L_e/(1+\gamma^2)]^m}{(m+1)^{3/2}}, \tag{2}$$

where $\gamma = z/z_0$, $z_0 = \pi w_0^2/\lambda$ is the Rayleigh length, and $L_e = (1-e^{-\alpha_0 L})/\alpha_0$.

During the fitting procedure (solid curves in Fig. 2), the values of I_0, L, α_0, z_0, and w_0 are fixed (their values are presented in the Experimental section, except α_0: $\alpha_0 = A_{800}\ln(10)/L$, A_{800} is the sample absorbance at 800 nm), while the parameters n_2 and β are left adjustable. The series in Eq. (2) is convergent for our data, and it is not necessary to sum infinity elements. The final index m value (m_f) was tested from 1 to 10. For $m_f \gtrsim 6$, the difference in β values caused by increasing one m_f unity was negligible when compared to the other parameters errors. We chose, therefore, the value 10 for the final m (i.e., 11 elements summation) to do the fittings. Moreover, some data fluctuation and asymmetries in baseline can occur in Z-scan experiments, mainly caused by laser instabilities, surface imperfections, or wedge in the sample [38]. In the case of Fig. 2, the baseline asymmetries are caused by instabilities in the system composed by the laser and Pockels cell: the pulse energy changes a little from the beginning ($z = -25$ mm) to the end ($z = 25$ mm) of the experiment. The errors of the n_2 and β values caused by these asymmetries are taken into account when we estimate the error from the fitting procedure ($\sim$10%).

Figure 3 presents the values of n_2 [see Fig. 3(a)] and β [see Fig. 3(b)] of all the ferrofluid samples, plotted as a function of the particle's diameter D_{XRD}. The experimental errors of n_2 and β were, mainly, originated by the measurement of I_0 and the fitting procedure error.

The real and imaginary parts of the third-order optical susceptibility, $\mathrm{Re}\chi^{(3)}$ and $\mathrm{Im}\chi^{(3)}$, can be calculated from the experimental values of n_2 and β, respectively [38]. Figures 4(a) and 4(b) present the values of $\mathrm{Re}\chi^{(3)}$ and $\mathrm{Im}\chi^{(3)}$ for all the samples, as a function of the particles' diameter D_{XRD}, respectively. The values of n_2 (and $\mathrm{Re}\chi^{(3)}$) are higher for the smallest and biggest particles. On the other hand, Fig. 3(b) [and Fig. 4(b)] shows a clear tendency of decreasing the value of β (and $\mathrm{Im}\chi^{(3)}$) as the particles' diameter decreases.

At this point it is important to check if the particles' coatings have any contribution to the nonlinear optical response of the ferrofluids, in the same experimental conditions of our experiments. We performed Z-scan experiments with saturated aqueous solutions of citric acid, dextran, and phosphatidylcholine; saturated solutions of chitosan in acetic acid; and pure oleic acid. These solutions did not present any detectable nonlinear optical response, within the limits of our experimental setup. We have evaluated that the n_2 (and β) values of these solutions are, at maximum, 20 (and 10) times smaller than those obtained for the ferrofluids. Moreover, as these solutions were saturated, the concentrations of the coating molecules in all the experiments performed are much higher than those in actual ferrofluids. As a consequence, solutions with smaller molecular concentrations would present even smaller contributions to n_2 and β measured. As dextran sulfate has a structure very similar to dextran, and aminosilane is constituted mainly by amine, it is reasonable to assume that these molecules (present in the ferrofluid coating) also did not present a nonlinear optical response in our experimental conditions. We conclude, therefore, that the values of the nonlinear refractive index and the two-photon absorption coefficient presented in Figs. 3 and 4 are from the magnetite core of the nanoparticles.

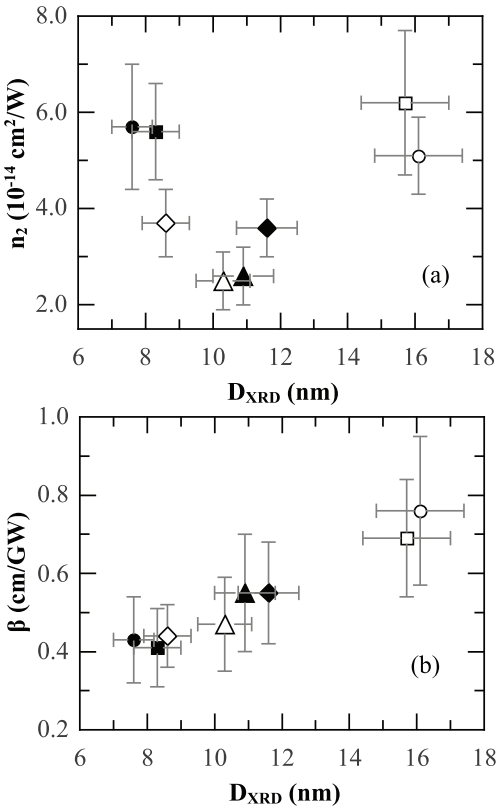

FIG. 3. Nonlinear refractive index n_2 (a) and two-photon absorption coefficient β (b) of the ferrofluids investigated, as a function of the particles' diameter D_{XRD}. Samples: • DXS, ■ DX, ◊ UCA, △ lipid, ▲ CT, ♦ amine, □ chitosan, ○ OS.

Let us now discuss the process involving the two-photon absorption inspecting the electronic orbital structure of magnetite. The TPA with photons of $\lambda = 800$ nm leads to an electronic transition of 3.10 eV, which can be associated to the intervalence charge transfer (IVCT) transition from the Fe^{2+} ions in the octahedral sites of magnetite to the Fe^{3+} ions in the tetrahedral sites [7]. This process is schematically illustrated in Fig. 5.

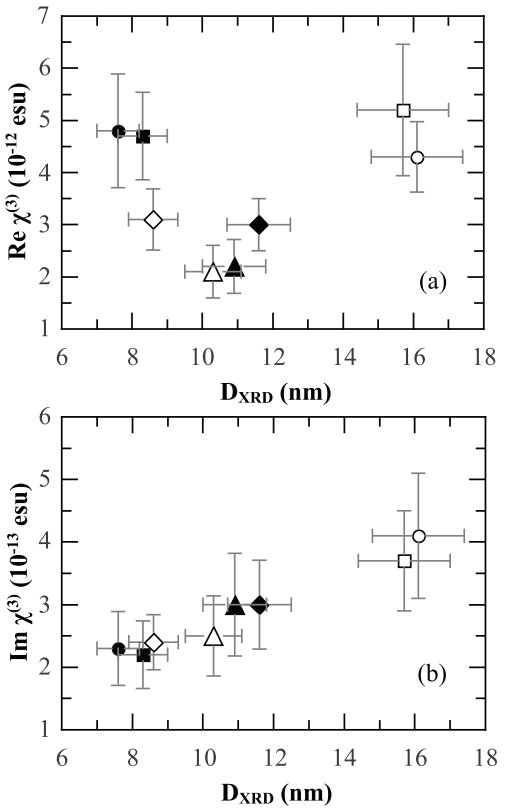

FIG. 4. Real $\mathrm{Re}\chi^{(3)}$ (a), and imaginary $\mathrm{Im}\chi^{(3)}$ (b) parts of the third-order optical susceptibility of the ferrofluids investigated, as a function of the particles' diameter D_{XRD}. Samples: • DXS, ■ DX, ◊ UCA, △ lipid, ▲ CT, ♦ amine, □ chitosan, ○ OS.

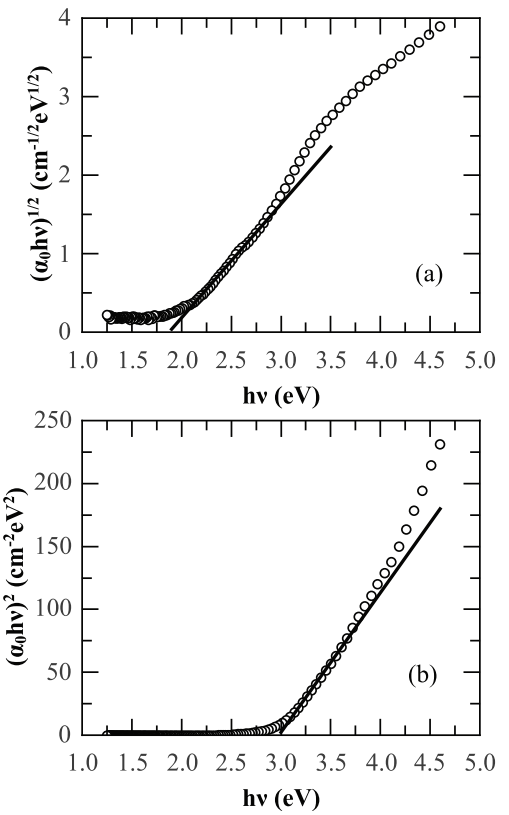

FIG. 6. Behavior of $(\alpha_0 h\nu)^{1/2}$ (a) and $(\alpha_0 h\nu)^2$ (b) as a function of the photon energy, for the determination of optical gap from indirect and direct transitions, respectively. UCA sample.

The electronic transitions in the magnetite nanoparticles can be experimentally evaluated through the determination of their optical gap. Figure 6 shows the experimental determination of the optical gap for the UCA sample. For parabolic bands model, the linear absorption coefficient is related to the optical gap (E_g) and photon energy ($h\nu$) according to the equation [52–54]

$$[\alpha_0 h\nu]^n = C(h\nu - E_g), \tag{3}$$

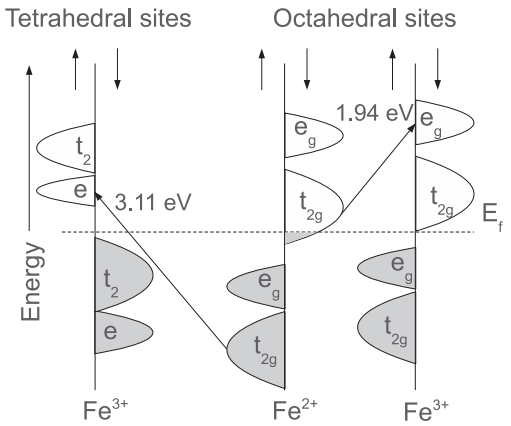

FIG. 5. Schematic diagram of the electronic orbital structure of Fe ions in magnetite. The 1.94-eV and 3.11-eV electronic transitions are indicated. Adapted from Fontijn *et al.* (1997) [7].

where C is a constant, $n = 2$ for direct allowed transitions, and $n = 1/2$ for indirect allowed transitions. The linear absorption coefficients, as a function of the photon energy, were calculated as $\alpha_0(h\nu) = A(h\nu)\ln(10)/L$, where $A(h\nu)$ is the absorbance measured by using the UV-vis spectrophotometry, and L is the thickness of the sample cell. According to Eq. (3), the extrapolation of the linear region of the curve represented in Fig. 6 to $\alpha_0 h\nu = 0$ allows the determination of E_g. The optical gap values obtained were (3.0 ± 0.1) eV and (1.9 ± 0.1) eV for the direct [see Fig. 6(b)] and indirect [see Fig. 6(a)] transitions, respectively. We repeated this measurement and analysis for all the other coated ferrofluids, and the results and conclusions are the same: all the ferrofluid samples presented the same E_g. This assures that we are dealing, essentially, with a characteristic of the magnetite core of the nanoparticles, regardless of the coating.

For short wavelengths [$h\nu \gtrsim 3.8$ eV, Fig. 6(b)], the data deviate from the linear curve. This indicates some contribution from the Rayleigh scattering to the data. However, even when we subtracted the estimated Rayleigh scattering contribution (see Fig. 1) from the absorbance data and recalculated the gaps, their values remain the same, within the error, which indicates that the Rayleigh scattering did not considerably affect our gap calculations.

Our values of E_g agree with those from the magnetite electronic transitions, reported by Fontijn *et al.* [7] (1.94 and 3.11 eV; see Fig. 5) through magneto-optical polar Kerr measurements in bulk single-crystalline Fe_3O_4 and Mg^{2+}- or

Al^{2+}-substituted Fe_3O_4. The experimental sensitivity of the UV-vis spectrophotometry method used in this work, however, could not evidence (eventual) small differences (smaller than 0.1 eV) in the optical gap of magnetite nanoparticles when their sizes change from 8 to 16 nm. On the other hand, the values of β measured with the Z-scan technique indicate a noticeable effect of the particles' diameter on the value of β, and consequently $\mathrm{Im}\chi^{(3)}$. This same behavior was observed in semiconductors CdSe, CdTe, Mn-doped ZnSe and Si nanoparticles [28–34], and metallic Ag nanoparticles [36], i.e., β (and $\mathrm{Im}\chi^{(3)}$) decreases as the particles' size decreases. It is worthwhile to stress that, in our case, we considered that the electronic transitions occurring due to the TPA in magnetite are IVCT from $[Fe^{2+}]$ to (Fe^{3+}) ions; this is not the case in semiconductors and metallic materials. Therefore, the theoretical models developed to explain the nanosize effects in semiconductors and metallic materials may not be applied to magnetite half metallic MNPs.

The decrease of β as the particles' diameter decreases may be due to an increase of the energy gap $t_{2g} \rightarrow e$ (see Fig. 5), or a change in the shape of the orbital itself, or both. Our measurements of E_g allow an evaluation of an eventual change in the energy gap. It is smaller than 3.5% between nanoparticles whose diameters change from 8 to 16 nm. The change in β for these nanoparticles is about 100%. This fact tends to support the idea that the nanosize effect is due to a modification of the shape of the orbitals involved in the electronic transition. Another aspect that could be considered here is that the magnetic nanoparticles have a spin-disordered layer around the spin-ordered core [55,56]. In our experiments the volume fraction of Fe was kept constant. A decrease of the particle's diameter, by a factor of 2, leads to an increase of the surface to volume ratio also by a factor of 2. If the core and the surface have different orbital structures, they may absorb light differently. Therefore, from one sample to another, the modification in the proportions of surface and core absorbers change, leading to different values of β as a function of the particles' diameter.

IV. CONCLUSION

We measured the nonlinear index of refraction and two-photon absorption coefficient of ferrofluids with magnetite nanoparticles as a function of the size and with different coatings, through the Z-scan technique, with femtoseconds light pulses ($\lambda = 800$ nm). The values of n_2 varied from 2.5×10^{-14} to 6.2×10^{-14} cm^2/W, and the values of β varied from 0.41 to 0.76 cm/GW. These values depend more significantly on the nanoparticles' size than on the particular coating employed to keep the colloidal stability. The two-photon absorption coefficient decreases as the particle diameter decreases, showing a nanosize effect. The optical gap for direct transition between the orbitals $t_{2g} \rightarrow e$ measured presented a value of $E_g = (3.0 \pm 0.1)$ eV, regardless of the particles' size. The decrease by a factor of 2 of β as the particle diameter decreases from 16 to 7.6 nm is interpreted invoking modifications in the orbital shape, corresponding to a nanosize effect, or even differences in the light absorption from the Fe in the surface, due to the spin-disordered layer, and in the core of the nanoparticles.

ACKNOWLEDGMENTS

We thank CNPq (Conselho Nacional de Desenvolvimento Científico e Tecnológico), FAPESP (Fundação de Amparo à Pesquisa do Estado de São Paulo), CAPES (Coordenação de Aperfeiçoamento de Pessoal de Nível Superior), and INCT-FCx (Instituto Nacional de Ciência e Tecnologia de Fluidos Complexos) for financial support.

[1] R. E. Rosensweig, in *Ferrohydrodynamics* (Courier Dover Publications, Mineola, NY, 1997), Chap. 1.
[2] N. Fauconnier, J. N. Pons, J. Roger, and A. Bee, J. Colloid Interface Sci. **194**, 427 (1997).
[3] R. Aquino, F. A. Tourinho, R. Itri, M. C. F. L. e Lara, and J. Depeyrot, J. Magn. Magn. Mater. **252**, 23 (2002).
[4] D. Maity and D. C. Agrawal, J. Magn. Magn. Mater. **308**, 46 (2007).
[5] J. A. Gomes, M. H. Sousa, F. A. Tourinho, R. Aquino, G. J. da Silva, J. Depeyrot, E. Dubois, and R. Perzynski, J. Phys. Chem. C **112**, 6220 (2008).
[6] E. J. Verwey, P. W. Haayman, and F. C. Romeijn, J. Chem. Phys. **15**, 181 (1947).
[7] W. F. J. Fontijn, P. J. van der Zaag, M. A. C. Devillers, V. A. M. Brabers, and R. Metselaar, Phys. Rev. B **56**, 5432 (1997).
[8] J. Tang, M. Myers, K. A. Bosnick, and L. E. Brus, J. Phys. Chem. B **107**, 7501 (2003).
[9] C. Rinaldi, T. Franklin, M. Zahn, and T. Cader, in *Dekker Encyclopedia of Nanoscience and Nanotechnology* (Taylor and Francis, New York, 2004), pp. 1731–1748.
[10] C. Scherer and A. M. Figueiredo Neto, Braz. J. Phys. **35**, 718 (2005).
[11] H. E. Horng, J. J. Chieh, Y. H. Chao, S. Y. Yang, Chin-Yih Hong, and H. C. Yang, Opt. Lett. **30**, 543 (2005).
[12] S. Pu, X. Chen, Y. Chen, Y. Xu, W. Liao, L. Chen, and Y. Xia, J. Appl. Phys. **99**, 093516 (2006).
[13] C. Z. Fan, G. Wang, and J. P. Huang, J. Appl. Phys. **103**, 094107 (2008).
[14] S. Monz, A. Tschöpe, and R. Birringer, Phys. Rev. E **78**, 021404 (2008).
[15] Y. Fainman, L. P. Lee, D. Psaltis, and C. Yang, *Optofluidics: Fundamentals, Devices, and Applications* (McGraw-Hill, New York, 2009).
[16] H. Schmidt and A. R. Hawkins, Nat. Photon. **5**, 598 (2011).
[17] M. F. da Silva and A. M. Figueiredo Neto, Phys. Rev. E **48**, 4483 (1993).
[18] J. E. Martin, K. M. Hill, and C. P. Tigges, Phys. Rev. E **59**, 5676 (1999).
[19] T. Kruse, H-G. Krauthäuser, A. Spanoudaki, and R. Pelster, Phys. Rev. B **67**, 094206 (2003).
[20] G. N. Rao, Y. D. Yao, Y. L. Chen, K. T. Wu, and J. W. Chen, Phys. Rev. E **72**, 031408 (2005).
[21] C. Rablau, P. Vaishnava, C. Sudakar, R. Tackett, G. Lawes, and R. Naik, Phys. Rev. E **78**, 051502 (2008).

[22] M. Adrian and L. E. Helseth, Phys. Rev. E **77**, 021403 (2008).
[23] B. Yu, C. Zhu, F. Gan, X. Wu, G. Zhang, G. Tang, and W. Chen, Opt. Mater. **8**, 249 (1997).
[24] M. Vivacqua, D. Espinosa, and A. M. Figueiredo Neto, J. Appl. Phys. **111**, 113509 (2012).
[25] R. W. Boyd, in *Nonlinear Optics* (Academic, New York, 1992), Chap. 1.
[26] J. Lenglet, A. Bourdon, J-C. Bacri, R. Perzynski, and G. Demouchy, Phys. Rev. B **53**, 14941 (1996).
[27] A. Yariv, in *Quantum Electronics*, 2nd ed. (Wiley, New York, 1989), Chap. 16.
[28] D. Cotter, M. G. Burt, and R. J. Manning, Phys. Rev. Lett. **68**, 1200 (1992).
[29] S.-C. Pu, M.-J. Yang, C.-C. Hsu, C.-W. Lai, C.-C. Hsieh, S. H. Lin, Y.-M. Cheng, and P.-T. Chou, Small **2**, 1308 (2006).
[30] L. A. Padilha, J. Fu, D. J. Hagan, E. W. Van Stryland, C. L. Cesar, L. C. Barbosa, C. H. B. Cruz, D. Buso, and A. Martucci, Phys. Rev. B **75**, 075325 (2007).
[31] G. S. He, K.-T. Yong, Q. Zheng, Y. Sahoo, A. Baev, A. I. Ryasnyanskiy, and P. N. Prasad, Opt. Express **15**, 12818 (2007).
[32] Y. Qu and W. Ji, J. Opt. Soc. Am. B **26**, 1897 (2009).
[33] C. Gan, M. Xiao, D. Battaglia, N. Pradhan, and X. Peng, Appl. Phys. Lett. **91**, 201103 (2007).
[34] R. Adamo, A. Anopchenko, P. Bettotti, M. Cazzanelli, E. D'Amato, N. Daldosso, L. Ferraioli, E. Froner, Z. Gaburro, R. Guider, S. M. Hossain, D. Navarro-Urrios, A. Pitanti, S. Prezioso, M. Scarpa, R. Spano, M. Wang, and L. Pavesi, Appl. Surf. Sci. **255**, 624 (2008).
[35] L. A. Padilha, G. Nootz, P. D. Olszak, S. Webster, D. J. Hagan, E. W. Van Stryland, L. Levina, V. Sukhovatkin, L. Brzozowski, and E. H. Sargent, Nano Lett. **11**, 1227 (2011).
[36] V. P. Drachev, A. K. Buin, H. Nakotte, and V. M. Shalaev, Nano Lett. **4**, 1535 (2004).
[37] M. Sheik-Bahae, A. A. Said, and E. W. Van Stryland, Opt. Lett. **14**, 955 (1989).
[38] M. Sheik-Bahae, A. A. Said, T. H. Wei, D. J. Hagan, and E. W. Van Stryland, IEEE J. Quantum Electron. **26**, 760 (1990).
[39] D. Espinosa, D. Soga, S. Alves, L. De Boni, S. C. Zílio, and A. M. Figueiredo Neto, J. Opt. Soc. Am. B **29**, 280 (2012).
[40] R. Fan, X. H. Chen, Z. Gui, L. Liu, and Z. Y. Chen, Mater. Res. Bull. **36**, 497 (2001).
[41] B. D. Cullity, in *Elements of X-Ray Diffraction*, 2nd ed. (Addison-Wesley, Reading, Massachusetts, 1978), Chap. 9.
[42] P. S. Haddad, T. M. Martins, L. D'Souza-Li, L. M. Li, K. Metze, R. L. Adam, M. Knobel, and D. Zanchet, Mater. Sci. Eng. C **28**, 489 (2008).
[43] A. V. Shulenina, M. V. Avdeev, V. L. Aksenov, A. A. Veligzhanin, Ya. V. Zubavichus, A. Hadju, and E. Trombacz, Mosc. Univ. Phys. Bull. **67**, 186 (2012).
[44] E. Tronc and D. Bonnin, J. Phys. Lett. **46**, 437 (1985).
[45] C. Groß, K. Büscher, E. Romanus, C. A. Helm, and W. Weitschies, Eur. Cells Mater. **3**, 163 (2002).
[46] V. K. Aswal, S. N. Chodankar, P. U. Sastry, P. A. Hassan, and R. V. Upadhyay, *Neutron and X-ray Scattering 2007: The International Conference*, AIP Conf. Proc. No. 989, edited by A. Ikram, A. Purwanto, Sutiarso, A. Zulfia, S. Hendrana, and Z. Nurachman (AIP, Melville, NY, 2008), p. 228.
[47] I. Rabias, M. Fardis, E. Devlin, N. Boukos, D. Tsitrouli, and G. Papavassiliou, ACS Nano **2**, 977 (2008).
[48] R. Ahmadi, H. Reza, M. Hosseini, A. Masoudi, H. Omid, R. Namivandi-Zangeneh, M. Ahmadi, Z. Ahmadi, and N. Gu, Colloids Surf. A: Physicochem. Eng. Aspects **424**, 113 (2013).
[49] K. Büsher, C. A. Helm, C. Gross, G. Glöckl, E. Romanus, and W. Weitschies, Langmuir **20**, 2435 (2004).
[50] M. Derakhshesh, M. R. Gray, and G. P. Dechaine, Energ. Fuel **27**, 680 (2013).
[51] C. Bohren and D. Huffman, *Absorption and Scattering of Light by Small Particles* (John Wiley and Sons, New York, 1983).
[52] J. Tauc, R. Grigorovici, and A. Vancu, Phys. Status Solidi **15**, 627 (1966).
[53] E. A. Davis and N. F. Mott, Philos. Mag. **22**, 0903 (1970).
[54] J. Tauc, *Amorphous and Liquid Semiconductors* (Plenum, New York, 1974).
[55] A. G. Roca, M. P. Morales, K. O'Grady, and C. J. Serna, Nanotechnology **17**, 2783 (2006).
[56] S. Linderoth, P. V. Hendriksen, F. Bødker, S. Wells, K. Davies, S. W. Charles, and S. Mørup, J. Appl. Phys. **75**, 6583 (1994).